2.B 24-Beam Implosion of Large-Aspect-Ratio Ar-DT Targets

As part of the program to assess the sensitivity of targets to irradiation uniformity, a number of different classes of DT-filled targets were irradiated under the most uniform conditions that could be achieved, i.e., where the RMS variation in energy deposition was less than 2% in all modes of order higher than eight. Their performance was compared with what one would expect from a perfectly symmetric implosion, deduced from the one-dimensional hydrocode *LILAC*. Target performance in these experiments was assessed through a consideration of the following: (1) analysis of the final core conditions, deduced from x-ray photography of the stagnated shell, (2) a measurement of the final core ρR, and (3) the use of a number of x-ray spectroscopic techniques, some of them novel. In this section, we describe one set of these experiments performed on large-diameter targets having initial aspect ratios as high as 275, at moderate intensities (1 to 4×10^{14} W/cm^2) with nanosecond pulses. In this range of intensity, inverse bremsstrahlung is the dominant mechanism of absorption, and with moderate energy loading of the order of 0.5 J/ngm, the shell achieves a peak velocity of the order of 1.5×10^7 cm/sec, before stagnating with a volumetric compression of the order of 300.

A typical x-ray photograph of one of these targets during irradiation is shown in Fig. 10. This particular target was overcoated with 5 μm of CH.

Fig. 10
X-ray micrograph of imploded argon-DT-filled target recorded in the 1 to 2 keV range (shot 7235). The target was a 400-μm-diameter glass microballoon with a 1.1-μm wall thickness and a 5-μm-thick plastic (CH) coating. It was filled with 20 atmospheres of DT and 2 atmospheres of argon. The total incident laser energy was 2.06 kJ (24 beams) with a pulse width of approximately 1 ns. The beams were focused 8 target radii behind target center.

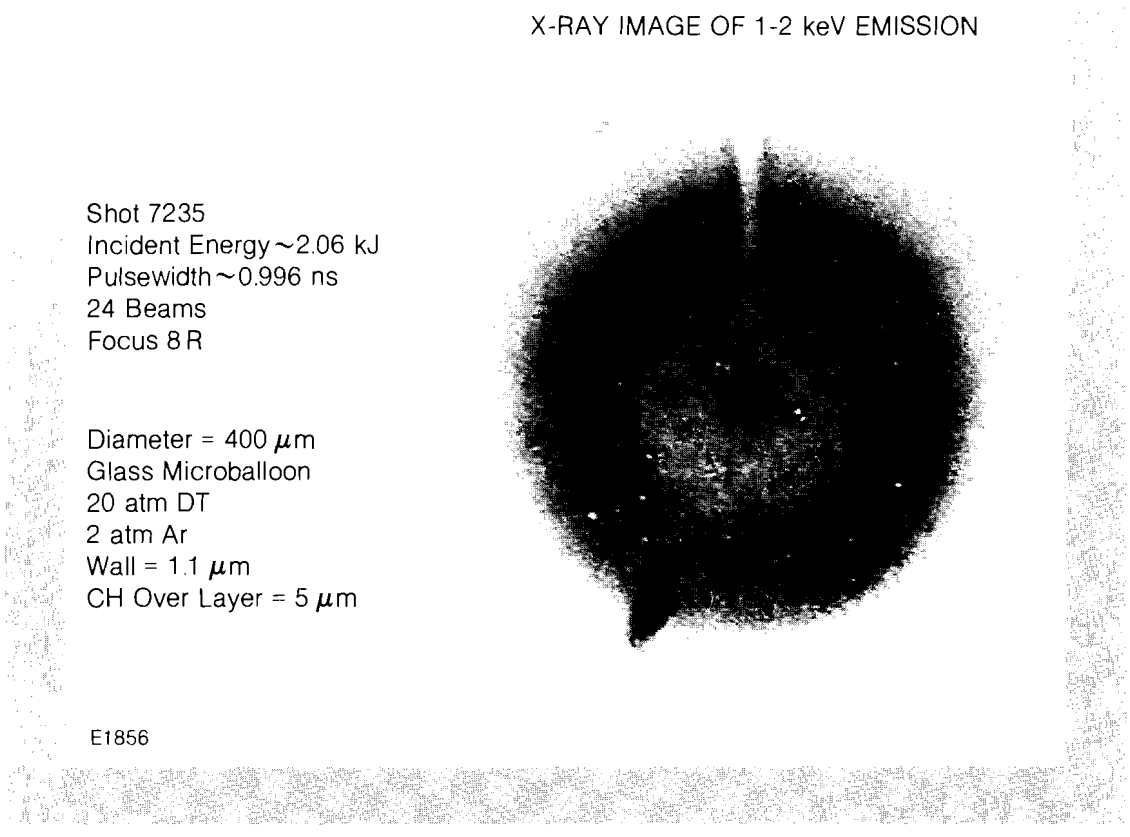

The extent of the ablation region during the laser pulse is shown by the radial extent of the annular emitting region. X-ray emission from the central core is clearly identified as being from Ar, Si, and Ca line emission, as will be shown later. The cooling effect of the 20-μm stalk can be clearly seen and the high-Z glass plug used to reseal the glass microballoon after Ar filling, can be identified.

The final ρR of the DT fuel was measured by a technique illustrated in Fig. 11. This technique analyzes the spectrum of deuterons and tritons elastically scattered off MeV neutrons in the core. The number of such scattered-reaction-product particles is directly proportional to the neutron yield, and to the density and the extent of the compressed core. CR-39 nuclear track detector material was used to detect the scattered deuterons and tritons. This material is a sensitive detector of high-velocity particles; the track diameter, under controlled etch conditions, is dependent on the original energy of the particle. The detector was maintained at atmospheric pressure in a special capsule deployed in the target chamber. A tantalum foil was used to discriminate against the effects of x-ray radiation and low-energy ions.

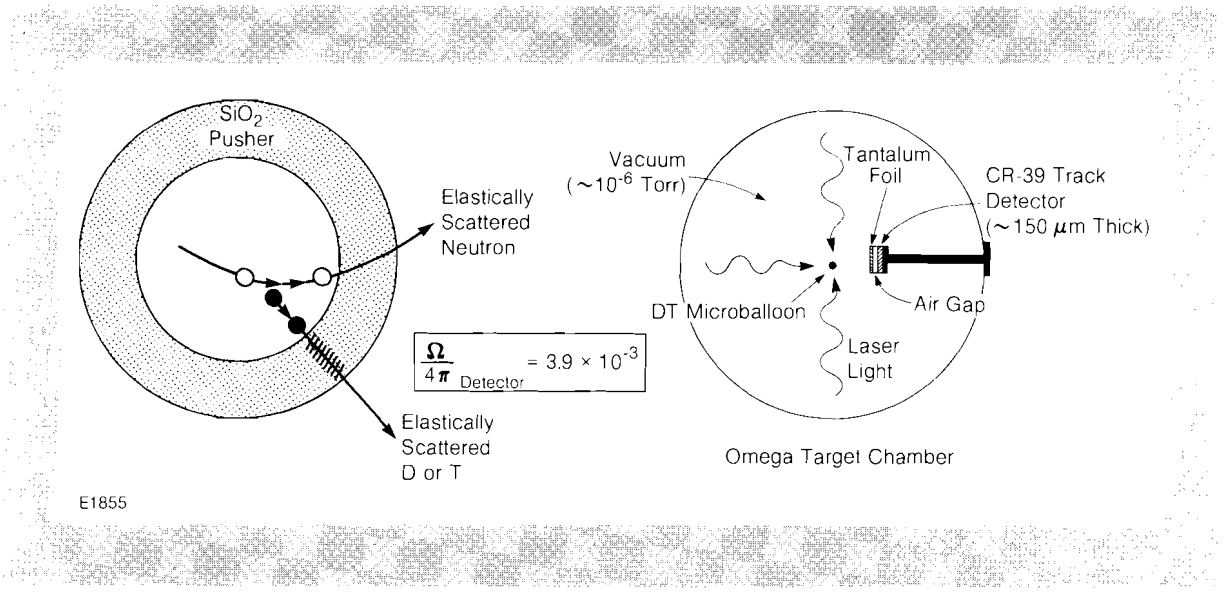

Fig. 11
Schematic illustration of the use of elastically scattered neutrons, deutrons, and tritons in the determination of compressed core conditions.

The thickness of the foil filter determines the range of deuterons and tritons which may be detected, and the use of several detectors with different filters permits us to determine the total, combined spectrum of deuteron and triton, as shown in Fig. 12. Discrimination against the 14-MeV protons is effectively made by utilizing 100-μm-thick plates of CR-39, in which the proton has little range. However, the scattered hydrogenic ions have sufficient energy to pass right through the detector providing coincident etched tracks on each side of the detector. Thus, the total recorded track spectrum for a typical Ar-DT shot is as shown in Fig. 13. Here the lower etched region shows the spectrum of coincident tracks resulting from deuterons and tritons, whereas the upper etched region shows the added counts from noncoincident tracks resulting primarily from 14-MeV protons. The resultant value of ρR deduced from this spectrum and from the known yield was 2.6×10^{-3} g/cm^2 with a statistical error of 15%.

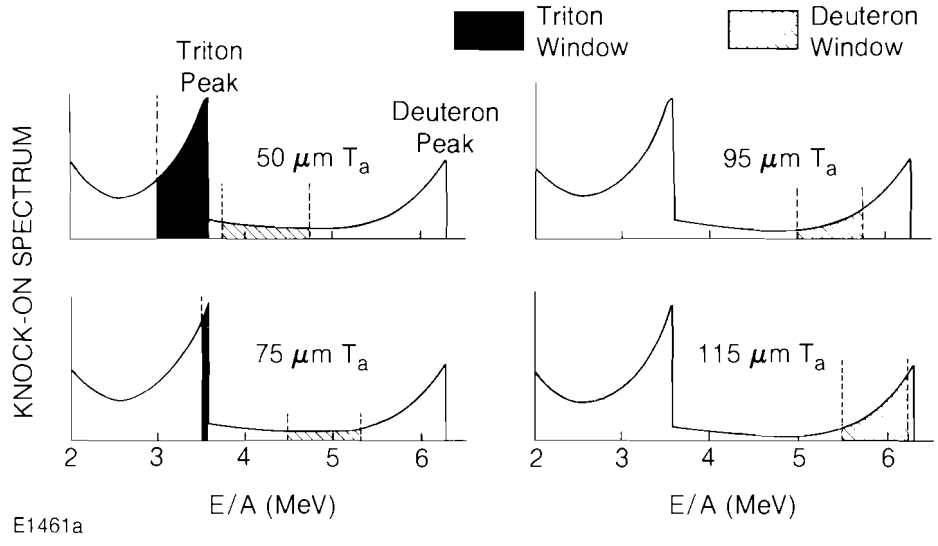

Fig. 12
Illustration of the effective response windows of various foil-filtered, CR-39 track detectors for elastically scattered core reaction products.

Shot 7219
Energy on Target = 2.15 kJ
Pulsewidth = 1044 ps
24 Beams
Focus = 8 R

Diameter = 414 μm
Wall = 0.84 μm
20 atm DT
2 atm Ar

$Y_n = 1.4 \times 10^8$

$\rho R = (2.6 \pm 0.4) \times 10^{-3}$ gm/cm^2

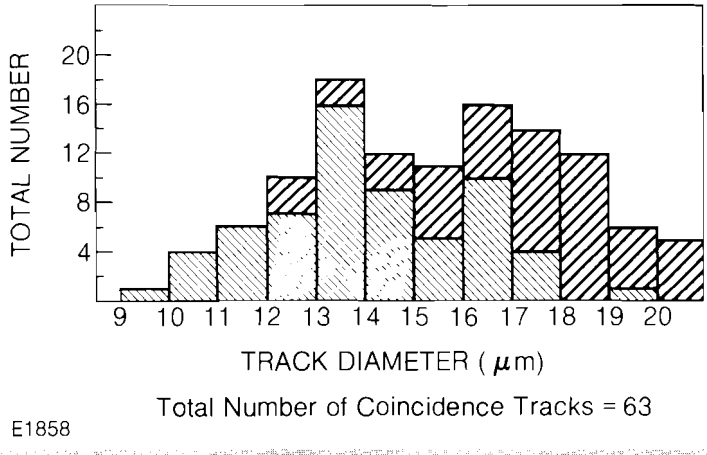

Fig. 13
Reaction-product track spectrum from shot 7219. The target was a 414-μm-diameter glass microballoon with 0.84-μm wall thickness. It was filled with 20 atmospheres of DT and 2 atmospheres of argon. The total incident laser energy was 2.15 kJ (24 beams) with a pulse width of 1.044 ns. The beams were focused 8 target radii behind the target center. The neutron yield was 1.4x10⁸.

Spectroscopic techniques provide an alternative approach to the direct measurement of ρR. Figure 14 shows a typical Ar spectrum from this type of target. Although the Ar-L_α line is optically thick in this range of ρ and ρR, the Stark broadening ~16eV of the L_β line (although not totally optically thin) would indicate a maximum Ar density

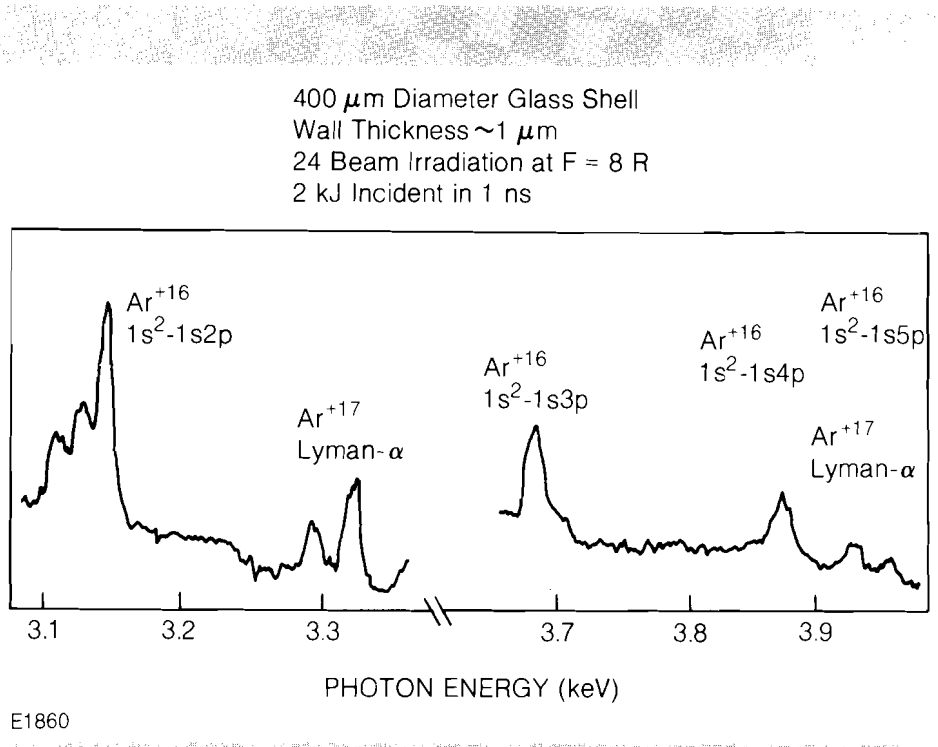

Fig. 14
Argon x-ray line emission spectrum from the target used in shot 7219 (Fig. 13). Detailed analysis of the lineshape of the argon Lyman-β emission permits a density of 0.7 g/cm³ to be deduced.

of 0.7 g/cm³. An estimate of the opacity effect has recently been formulated which predicts that it has at best a 10% effect on the calculated value of the density. This formalism also provides an estimate of the Ar $\rho R \sim 2.5 \times 10^{-3}$ g/cm².

These values are supported by monochromatic x-ray microscopy of the extent of the Ar emission region obtained with the instrument shown in Fig. 15. A fine (2d = 3000 Å) free-standing gold transmission grating, together with a 100-μm slit, is imposed within the optical path of a Kirkpatrick–Baez microscope providing two-dimensional microscopic images of the emitting regions of specific lines. Thus, each mirror combination of the Kirkpatrick–Baez microscope produces a conventional zero-order image resulting from undispersed x-rays in the microscope. On each side of the zero-order image are displayed the first- and second-order images of line emission emitted from the target. A typical image of an Ar-D_2 target is shown in Fig. 16. The large circular area of diffuse x-ray emission in the center of the image results from the deliberately overexposed zero-order image. On either side can be seen distinct images of the $\simeq$ 4keV Ar resonance line emission, and also that of the Si x-ray emission originating from the core of the target. The spatial extent of the Ar emission is ~40 μm, whereas the Si emission originates from a somewhat larger region (~80 μm), as one would expect. These photographs of the emitting region of the Ar imply final values of the Ar density radius product $\sim 2.5 \times 10^{-3}$ g/cm², in close agreement with the value determined for DT from scattered reaction product spectrometry.

Similar values for the extent of the emitting region of x-rays from the diagnostic gas in the core can be deduced from space-resolved x-ray

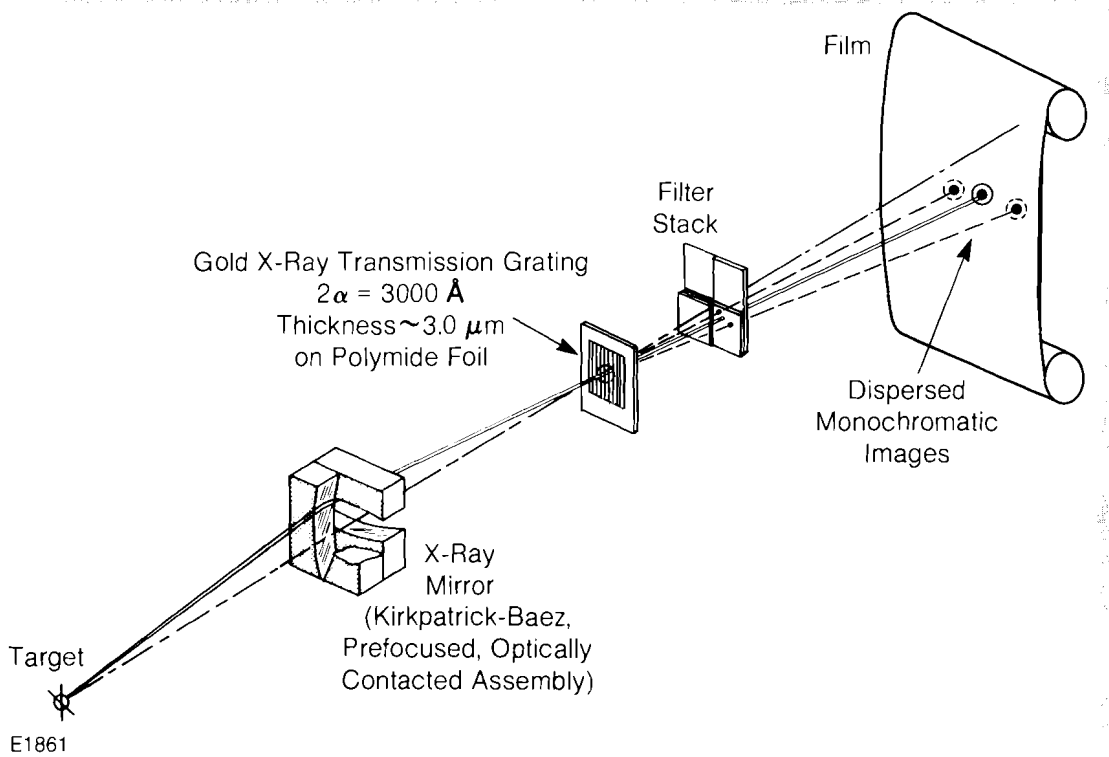

Fig. 15 Schematic of the use of a soft x-ray transmission grating (supplied by NLUF users) with the LLE K-B x-ray microscopy to obtain spatially and spectrally resolved images of imploded targets.

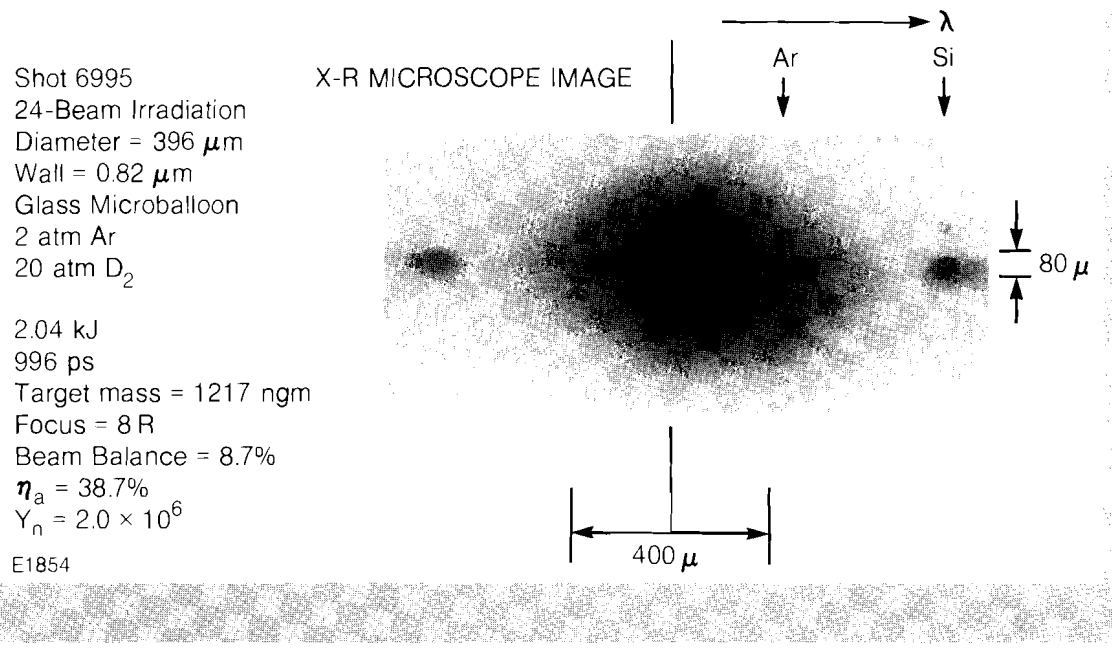

Fig. 16 X-ray images of an argon-D_2-filled target obtained with the system shown in Fig. 15.

spectroscopy. This is illustrated in Fig. 17 which shows the spatial profiles of Si- and Ne-L_α lines from the compressed core of a 400-μm-diameter D_2 Ne-filled target. As the figure demonstrates, the spatial extent of the Ne is ~50 μm, whereas Abel inversion of the Si emission yields a ring having a diameter of approximately 100 μm.

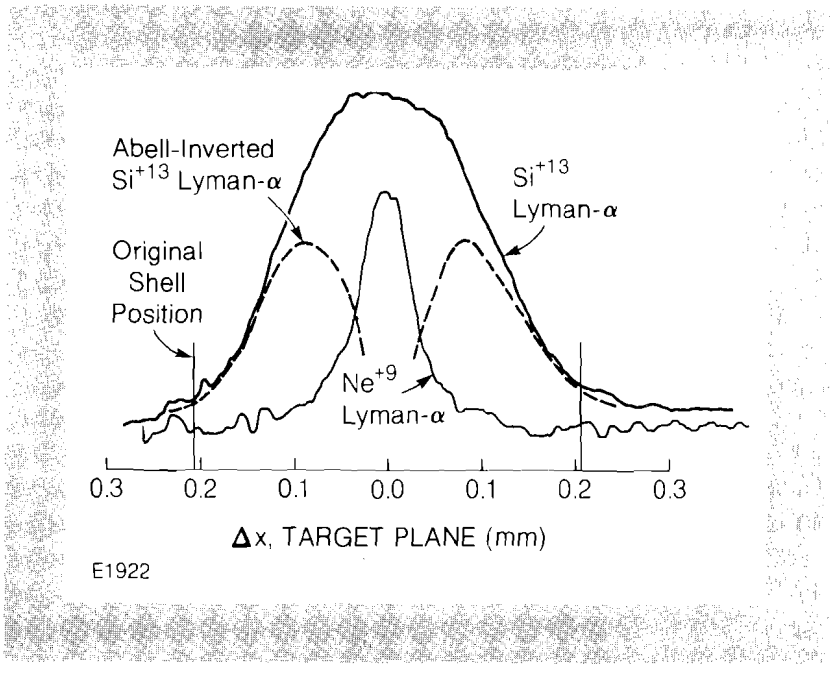

Fig. 17
Spatially resolved x-ray line emission from various target components in a D_2 + 10% neon-filled target.

The experimentally determined parameters of the final core state and the predictions of the one-dimensional hydrocode *LILAC* are in reasonable agreement. Table 1 shows experimentally and theoretically determined values for the Ar-DT target shot illustrated in previous figures. The

SHOT 7219

LASER PARAMETERS		TARGET PARAMETERS	
Input Power: 2.1 TW		Fuel: DT (20 atm); Ar (2 atm)	
Pulse Length: 1.04 ns		201 μm radius	
		Pusher: 0.84 μm glass	
	Experiment		*LILAC* Simulation
Absorption	0.37		0.36
Neutron Yield Y_n	2.0×10^8		1.4×10^8
DT density (g/cm^3)	0.7		1.0
Ar density (g/cm^3)	0.7		1.0
R core (μm)	35		30.0
ρR (DT) (mgm/cm^2)	2.6 ± 0.4		3.0
ρR (Ar) (mgm/cm^2)	2.5 ± 0.5		3.0
ρR (Total) (mgm/cm^2)	5.1		6.0

E2157

Table 1
Comparison of OMEGA experimental results with LILAC simulation of large-aspect-ratio target implosion. The comparison is made using the laser and target parameters from shot number 7219.

one-dimensional hydrosimulation was made on the basis of predominantly inverse bremsstrahlung absorption with a flux-limited thermal transport model (f = 0.05), and with a deposition into fast electrons of 10% of that energy reaching the critical density surface. This implied, typically, that no more than 2% of the absorbed energy would be deposited into fast electrons. As we can see, there is substantial agreement between the measured absorption and the neutron yield predictions. The experimentally determined values of the final core density and radius are well bracketed by the predictions of the one-dimensional code. The variability in the final values of the core density and radius predicted from *LILAC* arises as a consequence of the rapid variation of ρR around the time of peak compression. The strong calculated variation in ρR in this simulation is shown in Fig. 18. The difference between the measured total ρR value and that predicted at the time of peak neutron production is a factor of 2. The difference in time between these two points on the ρR curve is ~100 ps. Although the one-dimensional code predicts the experimentally determined values of the core density and radius very well, the rapid changes in these parameters around peak compression emphasizes the need for more detailed time-resolved diagnostics of the final core state.

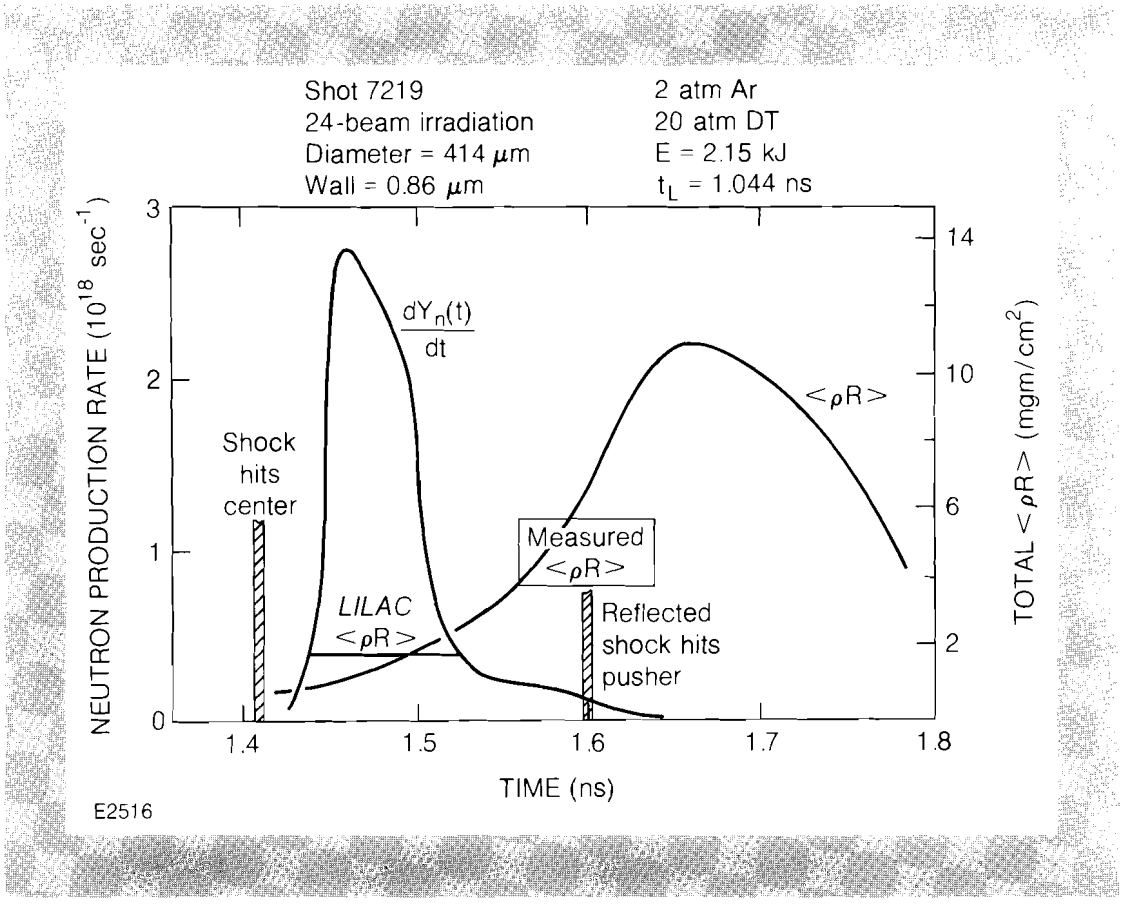

Fig. 18
Calculated time-histories of neutron yield and core <ρR> for shot 7219 (also discussed in Figs. 13 and 14).

We have described some initial experiments on Ar-seeded, large-diameter, high-aspect-ratio, DT-filled, glass microballoons irradiated with nanosecond pulses from the 24-beam OMEGA facility at moderate intensities. Measurements of the final core conditions through x-ray microscopy, core-reaction-product spectrometry, and time- and space-re-